

Large quadrupole deformation in ^{20}Ne challenges rotor model and modern theory: urging for α clusters in nuclei

C. V. Mehl,¹ J. N. Orce,^{1, 2,*} C. Ngwetsheni,¹ P. Marević,³ B. A. Brown,⁴ J. D. Holt,^{5, 6} M. Kumar Raju,^{1, †} E. A. Lawrie,^{7, 1} K. J. Abrahams,¹ P. Adsley,^{7, 8} E. H. Akakpo,¹ R. A. Bark,⁷ N. Bernier,^{1, 2} T. D. Bucher,^{1, 7} W. Yahia-Cherif,⁹ T. S. Dinoko,^{1, 7, ‡} J.-P. Ebran,¹⁰ N. Erasmus,¹ P. M. Jones,⁷ E. Khan,¹¹ N. Y. Kheswa,^{7, 1} N. A. Khumalo,^{1, 7} J. J. Lawrie,^{1, 7} S. N. T. Majola,^{12, §} K. L. Malatji,^{1, 7} D. L. Mavela,¹ M. J. Mokgolobotho,¹ T. Nikšić,³ S. S. Ntshangase,¹² V. Pesudo,^{1, 7} B. Rebeiro,¹ O. Shirinda,^{7, 8} D. Vretenar,³ and M. Wiedeking⁷

¹Department of Physics & Astronomy, University of the Western Cape, P/B X17, Bellville 7535, South Africa

²National Institute for Theoretical and Computational Sciences (NITheCS), South Africa

³Department of Physics, Faculty of Science, University of Zagreb, Bijenička c. 32, 10000 Zagreb, Croatia

⁴Department of Physics & Astronomy and National Superconducting Cyclotron Laboratory, Michigan State University, East Lansing, MI 48824-1321, USA

⁵TRIUMF, 4004 Wesbrook Mall, Vancouver, BC V6T 2A3, Canada

⁶Department of Physics, McGill University, Montréal, QC H3A 2T8, Canada

⁷iThemba LABS, National Research Foundation, P.O. Box 722, Somerset West 7129, South Africa

⁸Department of Physics, Stellenbosch University, P/B X1, 7602 Matieland, South Africa

⁹Université des Sciences, Faculté de Physique, BP 32 El-Alia, 16111 Bab-Ezzouar, Alger, Algeria

¹⁰CEA, DAM, DIF, F-91297 Arpajon, France

¹¹Institut de Physique Nucléaire, IN2P3-CNRS, Université Paris-Saclay, F-91406 Orsay Cedex, France

¹²Department of Physics & Engineering, University of Zululand, P/B X1001, KwaDlangezwa 3886, South Africa

(Dated: November 19, 2024)

The spectroscopic quadrupole moment of the first excited state, $Q_S(2_1^+)$, at 1.634 MeV in ^{20}Ne was determined from sensitive reorientation-effect Coulomb-excitation measurements using a heavy target and safe energies well below the Coulomb barrier. Particle- γ coincidence measurements were collected at iThemba LABS with a digital data-acquisition system using the AFRODITE array coupled to an annular, doubled-sided silicon detector. A precise value of $Q_S(2_1^+) = -0.22(2)$ eb was determined at backward angles in agreement with the only safe-energy measurement prior to this work, $Q_S(2_1^+) = -0.23(8)$ eb. This result adopts $1\hbar\omega$ shell-model calculations of the nuclear dipole polarizability of the 2_1^+ state that contributes to the effective quadrupole interaction and determination of $Q_S(2_1^+)$. It disagrees, however, with the ideal rotor model for axially-symmetric nuclei by almost 3σ . Larger discrepancies are computed by modern state-of-the-art calculations performed in this and prior work, including *ab initio* shell model with chiral effective interactions and the multi-reference relativistic energy density functional (MR-EDF) model. The intrinsic nucleon density of the 2_1^+ state in ^{20}Ne calculated with the MR-EDF model illustrates the presence of α clustering, which explains the largest discrepancy with the rotor model found in the nuclear chart and motivates the explicit inclusion of α clustering for full convergence of $E2$ collective properties.

Keywords: spectroscopic quadrupole moment, nuclear dipole polarizability, safe Coulomb excitation, $B(E2)$ values, photo-absorption cross sections, *ab initio*, mean-field and shell models, α clusters

Light-ion collisions (LIC) is a novel avenue of research at modern heavy-ion collision (HIC) facilities [1] aimed at understanding the general hydrodynamic behaviour of the quark-gluon plasma and the geometry of light nuclei, where varying shapes — e.g., α clusters and triaxiality fluctuations — may be inferred from the overlap region or centrality [2] of the two colliding nuclei [3, 4]. The application to smaller symmetric systems — e.g., $^{16}\text{O} + ^{16}\text{O}$ and $^{20}\text{Ne} + ^{20}\text{Ne}$ — has an advantage with respect to typical Pb+Pb, Au+Au and other HICs involving protons

because of the less sensitivity to spatial fluctuations in the proton and a better defined centrality [5]. One of the most crucial shapes concerns the nucleus ^{20}Ne [6], where a cluster formation — the so-called bowling pin — is expected from an increased incoherent cross section relative to an assumed spherical shape [7]. The initial geometry of the nucleus before collision is crucial, nonetheless, to assess nuclear clusters in future LIC measurements [4].

A long-standing challenge to nuclear structure physics concerns the large quadrupole deformation of the first excited state, $J^\pi = 2_1^+$, in ^{20}Ne [8] — where J is the angular momentum and π the parity — which arguably presents the most extreme quadrupole shape in the Segré chart. With only two protons and two neutrons above the shell closure with magic number 8, a favorable prolate deformation at the beginning of the sd shell is expected from the relatively sharper decrease in energy of the $\frac{1}{2}[220]$ single-particle Nilsson orbit as a function of deformation [9]. However, the magnitude of the quadrupole de-

* Corresponding author: jnorce@uwc.ac.za; coulex@gmail.com; <http://nuclear.uwc.ac.za>; <https://github.com/UWCNuclear>

† Present address: Department of Physics, GITAM School of Science, GITAM University, Visakhapatnam 530045, India

‡ Present address: National Metrology Institute of South Africa, P/B X 34, Lynnwood Ridge, Pretoria 0040, South Africa.

§ Present address: Department of Physics, University of Johannesburg, P/B 524, Auckland Park, 2006, South Africa

formation cannot be reproduced by the rotational model of Bohr and Mottelson [9] nor can it be computed by the shell [10, 11], mean-field [12–14], resonating group method [15] and multi-configurational [16] models. It further questions the simple picture provided by the N_pN_n scheme [17]. With $N_p(N_n)$ being the number of valence proton (neutron) pairs, a larger number of valence nucleons in midshell should produce larger deformations within a major shell.

In more detail, the spectroscopic quadrupole moment in the laboratory frame, $Q_s(J)$, can be determined for a nuclear state with $J \neq 0, \frac{1}{2}$ using the reorientation effect (RE) arising from the hyperfine interaction between Q_s and the time-dependent electric-field gradient generated by the projectile (P) and target (T) during the scattering process [18–20]. Assuming an axially-symmetric rotor, the intrinsic quadrupole moment of a nucleus in the body-fixed frame, Q_0 , can be determined from the reduced transition probability connecting the 0_1^+ ground and 2_1^+ states with an electric quadrupole (E2) operator, or $B(E2; 0_1^+ \rightarrow 2_1^+)$ value [9], as

$$Q_0 = \left(\frac{16\pi}{5} B(E2; 0_1^+ \rightarrow 2_1^+) \right)^{1/2}. \quad (1)$$

For $J^\pi = 2_1^+$ and $K = 0$ (e.g., ground-state band), where K is the projection of J onto the symmetry axis, $Q_s(2_1^+)$ and Q_0 can be related by

$$Q_s(2_1^+) = \frac{3K^2 - J(J+1)}{(2J+3)(J+1)} Q_0 = -2/7 Q_0, \quad (2)$$

where $Q_s(2_1^+) < 0$ for prolate and $Q_s(2_1^+) > 0$ for oblate deformations.

Nuclear interference may substantially affect the measurement of $Q_s(J)$ values, a common scenario in most of the first RE measurements carried out in the 1960s and 1970s [10]. The nucleus ^{24}Mg provides one of the most dramatic cases [10], where a very large $Q_s(2_1^+) = -24.3 \pm 3.5$ eb was determined [21], and soon disregarded by some of the same authors [22] and other groups [23] because of the very close distance between the colliding nuclei. For negligible nuclear contributions, Spear's systematic study of $Q_s(2_1^+)$ values in *sd*-shell nuclei [10] suggests a minimum safe distance of closest approach between nuclear surfaces of $S(\vartheta)_{min} \geq 6.5$ fm, where

$$\begin{aligned} S(\vartheta) &= \frac{e^2 Z_P Z_T}{8\pi\epsilon_0 T_{lab}} (1 + A_P/A_T) [1 + \text{cosec}(\vartheta/2)] \\ &\quad - 1.25(A_P^{1/3} + A_T^{1/3}) \text{ fm}. \end{aligned} \quad (3)$$

Here, ϑ is the scattering angle in the center-of-mass frame, Z and A the proton and mass number, respectively, and T_{lab} the kinetic or beam energy in the laboratory frame. Prior to this work, three RE Coulomb-excitation measurements were carried out in ^{20}Ne [24–26]. Two of the previous RE measurements, yielding $Q_s(2_1^+) = -0.24(3)$ eb [24] and $Q_s(2_1^+) = -0.20(5)$

eb [26], were carried out at exceedingly high T_{lab} energies, with $S(\vartheta)_{min}$ as low as 3.8 and 4.2 fm, respectively. The third RE measurement by Schwalm and collaborators was performed using a ^{20}Ne gas target at a safe $S(\vartheta)_{min} = 7.1$ fm, yielding $Q_s(2_1^+) = -0.23(8)$ eb. These RE measurements give a weighted average of $Q_s(2_1^+) = -0.23(3)$ eb, which is the accepted value in the National Nuclear Data Center (NNDC) [10]. Because of the relatively small Z and radius R , this represents the largest quadrupole (prolate) deformations in the nuclear chart with a quadrupole parameter of $\beta_2 = 0.96(11)$ [9].

It is interesting to compare the $Q_s(2_1^+)$ value determined with the RE and the one extracted from the rotational model [9], $Q_s(2_1^+)_{B(E2)}$, using Eqs. 1 and 2, by defining the spectroscopic quadrupole ratio [27–29],

$$r_q := \left| \frac{Q_s(2_1^+)}{Q_s(2_1^+)_{B(E2)}} \right|. \quad (4)$$

Data show $r_q \approx 1$ for good rotors in the rare-earth and $A \sim 180$ regions, while $r_q = 0$ is expected for an ideal vibrator ($Q_s(2_1^+) = 0$) [9]. With $Q_s(2_1^+)_{B(E2)} = \pm 0.165(4)$ eb [10, 30–32], an anomalously large $r_q(2_1^+) = 1.39(49)$ is determined in ^{20}Ne considering the only safe RE measurement. As already stated in Spear's 1981 review article [10], a new measurement of the $Q_s(2_1^+)$ value in ^{20}Ne was desirable. We present it here from a safe, precise and sensitive RE measurement.

Coulomb-excitation measurements have been carried out at iThemba LABS using the $^{194}\text{Pt}(^{20}\text{Ne}, ^{20}\text{Ne}^*)^{194}\text{Pt}^*$ reaction at a safe energy of 71.3 MeV and a digital DAQ system based on 100 MHz Pixie-16 modules from XIA LLC [33]. Pure beams of $^{20}\text{Ne}^{4+}$ ions at $\approx 1 \times 10^9$ pps were extracted from a 99.99%-enriched ^{20}Ne gas bottle and accelerated with the $K = 200$ separated sector cyclotron (SSC) onto a 95%-enriched ^{194}Pt target of 1.2 mg/cm^2 thickness. The scattered ions were detected using an annular, double-sided silicon detector (S3-type from Micron Semiconductors [34]) comprising 24 rings and 32 sectors [35] and mounted upstream at 27.5 mm from the target position and perpendicularly aligned with the beam axis. The scattering θ angles in the laboratory frame ranged between 128.1° and 157.3° , corresponding to $S(\vartheta) \approx 7.5$ and 6.9 fm, respectively. Gamma rays were collected with the AFRODITE array [36] comprising eight HPGe clover detectors at a distance of 19.6 cm between target and Ge crystals.

A low background γ -ray spectrum is achieved by collecting particle- γ coincidence events, which require both a γ and a particle hit within a coincidence time window of approximately 600 ns. A gate outside this prompt window was used for background subtraction. The particle hit was defined by a signal in one θ ring and one ϕ sector. A broad particle energy gate covering the range of the scattered $^{20}\text{Ne}^{4+}$ ions was also implemented. When multiple γ -ray events were detected in crystals within the

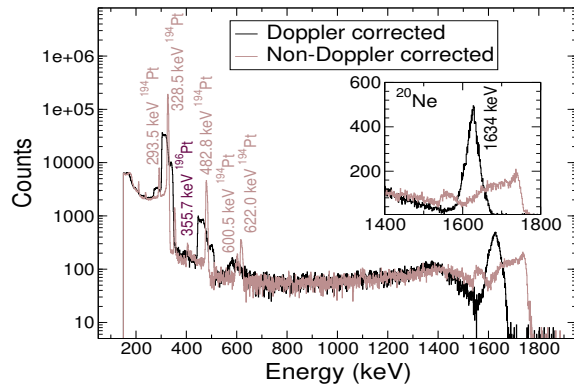


FIG. 1. Doppler (black) and non-Doppler (brown) corrected γ -ray energy spectra in log- y scale for the $^{194}\text{Pt}(^{20}\text{Ne}, ^{20}\text{Ne}^*)^{194}\text{Pt}^*$ reaction at 71.3 MeV. The inset shows the 1634-keV peak in ^{20}Ne in a linear scale.

same clover, the crystal with the highest deposited energy was used to Doppler correct the add-back energy of the detected γ ray. Figure 1 shows the resulting Doppler and non-Doppler corrected γ -ray energy spectra in coincidence with all rings. Total counts of $N_\gamma^P = 19523(953)$ and $N_\gamma^T = 882606(29334)$, respectively, for the 1634- and 328-keV γ rays depopulating the 2_1^+ states in ^{20}Ne and ^{194}Pt were measured.

The Coulomb-excitation analysis was performed using the semi-classical coupled-channel least-squares codes GOSIA and GOSIA2 [37, 38]. The integration of γ -ray yields accounts for detector angular limits, beam energy losses [39] and the solid angle subtended by the silicon detector. The effect of higher-lying states in ^{20}Ne was estimated using GOSIA and considered negligible ($<0.1\%$). Integrated yields for each data set are constrained by available spectroscopic information concerning level lifetimes, branching ratios and matrix elements for all significant couplings up to the 3^-_1 states in ^{20}Ne [40] and ^{194}Pt [40, 41]. Further corrections include γ -ray efficiencies with standard ^{152}Eu and ^{56}Co calibration sources ($\varepsilon_\gamma^P = 145.3(4.4)$ and $\varepsilon_\gamma^T = 344.5(6.9)$), internal-conversion processes [42] and angular-distribution attenuation factors for the finite size of the detectors [37]. As shown in Fig. 2, experimental γ -ray yields per 4 rings were rebinned to obtain 6 data points and compared with integrated yields calculated with GOSIA, which were normalized independently to the experimental yields in the projectile and target. The shape of the angular distributions predicted by GOSIA for both ^{20}Ne and ^{194}Pt are in agreement with experiment, and follow similar trends to those predicted by $d\sigma_{E2} = P d\sigma_R$, where P is the probability of exciting the 2_1^+ state following the scattering process and σ_{E2} and σ_R are the Coulomb-excitation and Rutherford cross sections, respectively.

In order to determine the values of $\langle 2_1^+ || \hat{E}2 || 2_1^+ \rangle$ and $\langle 2_1^+ || \hat{E}2 || 0_1^+ \rangle$ that reproduce the experimental yields,

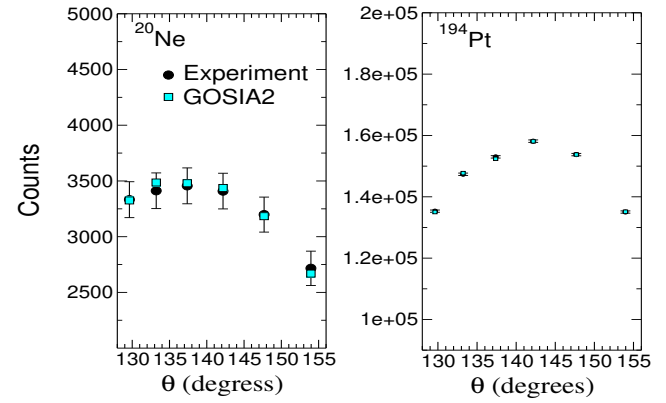


FIG. 2. Experimental and calculated (GOSIA) γ -ray yields as a function of particle angle θ for the de-excitation of the 2_1^+ states in ^{20}Ne (left) and ^{194}Pt (right).

the maximum likelihood approach [43] has been used. Figure 3 shows the χ^2 surface with 300×300 scanned points together with the corresponding $\chi^2 < \chi^2_{min} + 1$ for polarizability parameters of $k(2_1^+) = 1.7$ (left) and $k(2_1^+) = 0.6$ (middle), as discussed below. The data are normalised to the excitation of the ^{194}Pt target at a beam energy of 71.3 MeV using GOSIA2 [38], in conjunction with the accepted value of $\langle 2_1^+ || \hat{E}2 || 0_1^+ \rangle = 0.1825(44)$ eb in ^{20}Ne [44], which is in agreement with the transitional matrix element extracted from a recent high-precision lifetime measurement [45].

Further care must be taken in second-order Coulomb-excitation studies of light nuclei [18, 19, 46–48] where the nuclear electric dipole (E1) polarizability competes with the RE and may influence the determination of $B(E2)$ and $Q_s(2_1^+)$ values [20, 46]. The E1 polarizability is directly related to the static polarizability, $\alpha_{E1} = \frac{\mathbf{P}}{\mathbf{E}}$, where \mathbf{P} is the electric dipole moment induced in a nucleus by the time-dependent electric field \mathbf{E} of the partner. Consequently, E1 virtual excitations via high-lying states in the isovector giant dipole resonance (GDR) [49] — a collective motion of protons and neutrons out of phase characterized by the residual particle-hole interaction [50] — can polarize the ground and excited states of nuclei [46, 47, 51] without involving short-range Yukawa forces. Particularly, two-step processes of the type $0_1^+ \rightarrow 1_{GDR}^- \rightarrow 2_1^+$ can polarize the shape of the 2_1^+ state. This effect is characterized by the polarizability parameter κ , which accounts for deviations of the actual GDR effects to those predicted by the hydrodynamic model [52, 53] and is directly proportional to the polarization potential in modern Coulomb-excitation analysis codes [37, 54]. Collective properties may be enhanced for $\kappa > 1$, whereas shell effects can be inferred from $\kappa < 1$ [55–57]. Negligible polarizability effects were assumed in previous RE measurements of ^{20}Ne [24–26].

In order to assess the polarizability of the ground state, $\kappa(g.s.)$, in ^{20}Ne values of $\sigma(\gamma, p) = 165(25)$ MeV·mb

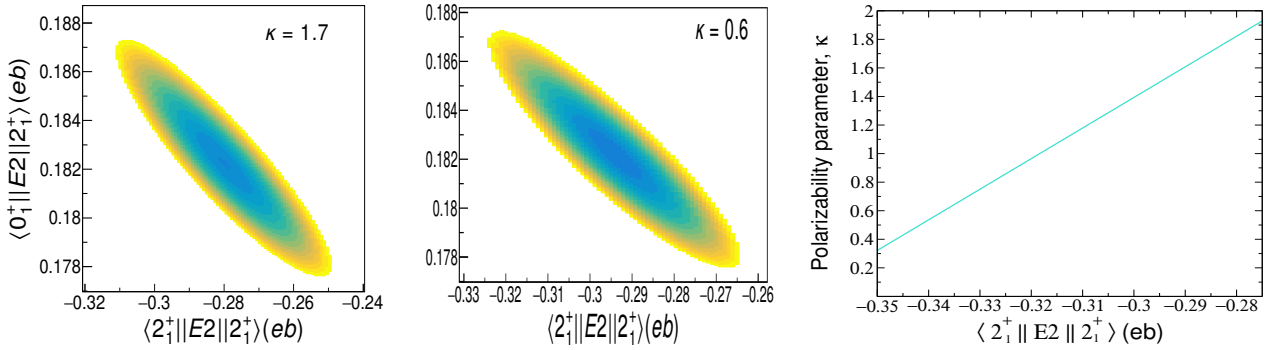


FIG. 3. Minimization of the χ^2 surface in the $\langle 2_1^+ \parallel \hat{E}2 \parallel 2_1^+ \rangle$ - $\langle 0_1^+ \parallel \hat{E}2 \parallel 2_1^+ \rangle$ 2D-plane for the ^{20}Ne projectile when combined with lifetime measurements [44] for $k(2_1^+) = 1.7$ (left) and $k(2_1^+) = 0.6$ (right). The data are normalised to the excitation of the ^{194}Pt target at a beam energy of 71.3 MeV using GOSIA2.

and $\sigma(\gamma, n) = 115(20)$ MeV·mb [58] were extracted in agreement with 1) the Thomas-Reiche-Kuhn (TRK) sum rule, $\sigma_{total}(E_\gamma) = 60 NZ/A = 300$ MeV [51, 59], and 2) proton emission being the predominant decay mode in $A = 4n$ self-conjugate nuclei [60]. A similar value of $\sigma(\gamma, p) = 160(80)$ MeV·mb has been observed [61]. The proton-neutron yield ratio, $r_{pn} = \sigma(\gamma, p)/\sigma(\gamma, n) \approx 165(25)/115(20) = 1.4(3)$, is in agreement with predictions based on the evaporation model of Blatt and Weisskopf [62], $r_{pn} = 1.3$ [60]. The resulting $\sigma_{-2} = 600(90)$ $\mu\text{b}/\text{MeV}$ [58] — which also includes (γ, α) contributions ($\approx 10\%$) — yields $\kappa(g.s.) = 1.7(3)$.

Shell-model (SM) calculations have additionally been performed in order to estimate $\kappa(g.s.)$ by combining the hydrodynamic model and the σ_{-2} value calculated from second-order perturbation theory [63],

$$\sigma_{-2} = \frac{16\pi^3 e^2}{9\hbar c} \frac{1}{2J_i + 1} \sum_n \frac{|\langle i \parallel \hat{E}1 \parallel n \rangle|^2}{E_\gamma}, \quad (5)$$

using the OXBASH SM code [64] with the WBP interaction [65] (the original *usd*) and the *spsdpf* model space. A value of $\kappa(g.s.) = 1.7$ is calculated in agreement with the experimental value. Details of the calculations are presented in Refs. [63, 66]. Assuming the same κ value for the 2_1^+ state, $\kappa(2_1^+) = 1.7$, the χ^2 minimization yields $\langle 2_1^+ \parallel \hat{E}2 \parallel 2_1^+ \rangle = -0.28(3)$ eb and $Q_s(2_1^+) = -0.21(2)$ eb, as shown in the left panel of Fig. 3.

Nonetheless, growing evidence suggests that κ may change from the ground to excited states [48, 66–69]. In fact, recent SM calculations yield a smaller value of $\kappa(2_1^+) = 0.6$ in ^{20}Ne [66], which is the adopted value in this work. Assuming $\kappa(2_1^+) = 0.6$, the χ^2 minimization shown in the middle panel of Fig. 3 yields similar values of $\langle 2_1^+ \parallel \hat{E}2 \parallel 2_1^+ \rangle = -0.29(3)$ eb and $Q_s(2_1^+) = -0.22(2)$ eb, which includes a 3% systematic error due to quantal effects. The right panel of Fig. 3 shows how $\langle 2_1^+ \parallel \hat{E}2 \parallel 2_1^+ \rangle$ shifts towards less prolate deformed shapes with increasing κ values.

This precise experimental result can now be used to

benchmark nuclear models and modern state-of-the-art theoretical calculations. As shown in the left panel of Fig. 4, this new result (circle for $Q_s(2_1^+) = -0.22(2)$ eb) presents a 2.735σ standard deviation with respect to the one extracted with the rotational model, $Q_s(2_1^+)_{B(E2)} = \pm 0.165(4)$ eb (square), which is arguably one of the largest deviations observed in nuclei. In addition, a large $r_q = 1.33(12)$ value is determined, which is clearly inconsistent with that expected for axially-symmetric rotors ($r_q = 1$). The right panel of Fig. 4 shows the r_q values for self-conjugate nuclei in the *sd* shell. In the SM calculations the r_q ratio does not depend on the effective charges. Values of $r_q \approx 1$ (diamonds) consistent with ideal rotors are computed with the WBP [65] and the *usdb* [70] interactions. More details on these SM calculations can be found in Ref. [71]. Nevertheless, large deviations from axial symmetry are evident at both extremes of the *sd* shell, suggesting a missing factor.

We have further performed *ab initio* calculations of energies and quadrupole moments in ^{20}Ne with the valence-space formulation of the in-medium similarity renormalization group (VS-IMSRG) [72–76]. In this approach, we construct a valence-space Hamiltonian, based on two-(NN) and three-nucleon (3N) forces from chiral effective field theory. In particular we use the “EM1.8/2.0” and “PWA” NN+3N interactions [77–81] — the former of which reproduces ground-state and separation energies up to the tin region from constraints to only few-body data [80, 81] — as well as $N_2\text{LO}_{\text{sat}}$ [82] and $N_4\text{LO}$ local-non-local interaction of Ref. [83], which well reproduces radii to the nickel region [82, 84]. We use the Magnus procedure [72, 85] to decouple an *sd*–shell Hamiltonian as well as the ^{16}O core energy. The effects of 3N forces between the ^{20}Ne valence nucleons are included via the ensemble normal ordering technique [76]. Finally, we use the approximate unitary transformation to decouple a consistent *E2* valence-space operator [86], where no effective charges are used or needed, in principle. Similar results of $Q_s(2_1^+) \approx -0.12$ eb are computed, as shown in the left panel of Fig. 4 (left triangles). This underestima-

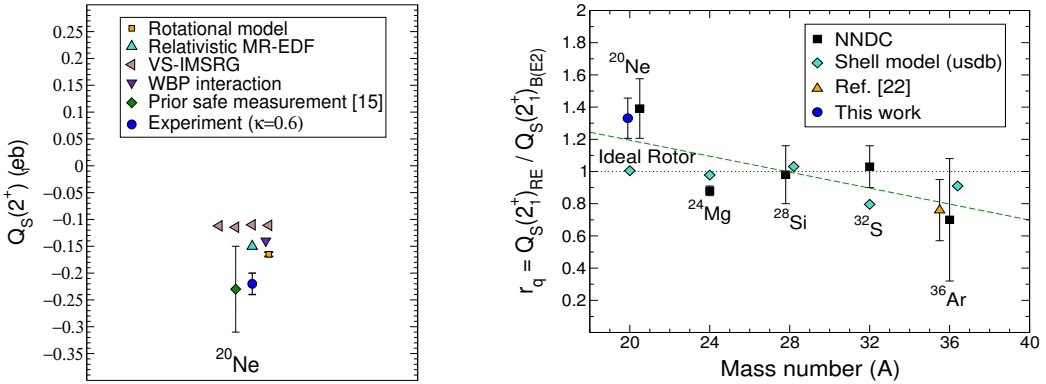


FIG. 4. The left panel shows experimental (rotational model, NNDC [10], previous work at safe energies [25] and current work for $\kappa = 0.6$) and theoretical (relativistic MR-EDF, VS-IMSRG and WBP) $Q_S(2_1^+)$ values in ^{20}Ne determined in the current work. For the VS-IMSRG calculations, the interactions are from left to right: PWA, N4LO, N2LO_{sat} and 1.8/2.0(EM). The right panel shows experimental and theoretical r_q values for self-conjugate nuclei within the sd -shell. For comparison, a linear regression to the most accurate data is shown by a dashed line.

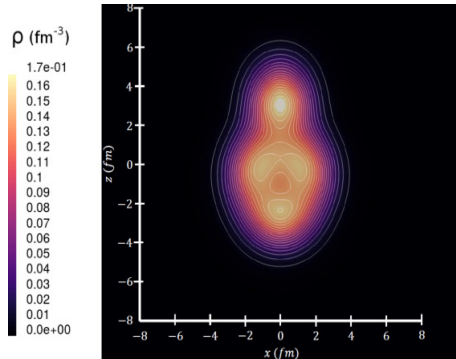


FIG. 5. Characteristic 2D intrinsic nucleon density of the 2_1^+ state in ^{20}Ne obtained with the MR-EDF model.

tion is not surprising as *ab initio* $E2$ transition rates are smaller than experimental ones, regardless of the initial interaction. This is likely due to the complex collective structures which require many particle-hole excitations to capture sufficiently and are a particular challenge for most methods [87–90]. Recent *ab initio* calculations in the neon isotopes with the projected generator coordinate method (PGCM) at a harmonic-oscillator basis size of $N_{\text{max}} = 4$ compute a larger value of $Q_S(2_1^+) = -0.183$ eb in ^{20}Ne [91]. Further studies of the origin and solution to this missing $E2$ strength are underway [92]. A slightly smaller value of $Q_S(2_1^+) = -0.143$ eb (down triangle in Fig. 4) is determined using further SM calculations with the WBP interaction and average effective charges in the sd -shell [70]. Similar results are obtained with the *usdb* and *usdc* interactions [93]. An ingredient that is not explicitly included in these *ab initio* and phenomenological interactions is α clustering.

Furthermore, we have performed multi-reference energy density functional (MR-EDF) calculations [94–97] based on the relativistic Hartree-Bogoliubov (RHB)

model [98, 99], using DD-PC1 functional [100] and separable pairing force [101] as global effective interactions. A total of 118 RHB states with a wide range of quadrupole and octupole deformations were first projected onto good values of angular momenta, particle numbers, and parity, and further mixed within the generator coordinate method framework [102, 103]. The calculated 2_1^+ state at 1.84 MeV exhibits a predominantly prolate $^{16}\text{O} + \alpha$ structure — the bowling pin shape shown in Fig. 5 — and decays to the ground state with a quadrupole transition strength of $B(E2; 0_1^+ \rightarrow 2_1^+) = 0.029 e^2 b^2$, in agreement with the experimental value. The corresponding $Q_S(2_1^+) = -0.15$ eb (triangle up on the left panel of Fig. 4) and $r_q = 0.97$ values are still too small compared with the experimental values determined in this work. Ongoing efforts to quantify the uncertainties of EDF-based models [97, 104, 105], particularly when extended to the multi-reference level, may enable a more rigorous test.

In conclusion, we present the most sensitive and precise reorientation-effect measurement of $Q_S(2_1^+) = -0.22(2)$ eb in ^{20}Ne up to date determined at safe energies with a heavy target and backward scattering angles through the χ^2 minimization of the integrated yields. We further quantify the competing second-order contribution arising from the electric dipole polarizability through $1\hbar\omega$ shell-model calculations. Large deviations from the rotor-model and various modern nuclear theory approaches are found, including *ab initio* and MR-EDF calculations done in this and prior work. The presence of a bowling pin shape for the 2_1^+ state in ^{20}Ne calculated with MR-EDF suggests that α clusters should be explicitly included in modern *ab initio* calculations [106]. In fact, a recent calculation by D. Lee reproduces the quadrupole moment presented here when considering α clusters in the interaction [107].

We acknowledge the accelerator group at iThemba LABS for masterful delivery of pure ^{20}Ne beams. CVM and JNO thank L. Gaffney, N. Warr, D. Lee, L. Robledo and the late D. Schwalm for interesting physics discussions and providing relevant information. This work was partly performed under the auspices of the U.S. Department of Energy by the Lawrence Livermore National Laboratory (LLNL) under contract No. DOE-AC52-07NA27344, the National Science Foundation (NSF) under grant PHY-1811855, and the South African National Research Foundation (NRF) under Grant 93500

-
- [1] “Light ion collisions at the LHC,” <https://indico.cern.ch/event/1436085> (Workshop at CERN, November 2024).
- [2] R. Aaij, C. A. Beteta, T. Ackernley, B. Adeva, M. Adinolfi, H. Afsharnia, C. A. Aidala, S. Aiola, Z. Ajaltouni, S. Akar, *et al.*, *Journal of Instrumentation* **17**, P05009 (2022).
- [3] J. Brewer, A. Mazeliauskas, and W. van der Schee, arXiv preprint arXiv:2103.01939 (2021).
- [4] G. Giacalone, B. Bally, G. Nijs, S. Shen, T. Duguet, J.-P. Ebran, S. Elhatisari, M. Frosini, T. A. Lähde, D. Lee, *et al.*, arXiv preprint arXiv:2402.05995 (2024).
- [5] C. Shen, URL <https://cds.cern.ch/record/2751277>.
- [6] J.-P. Ebran, E. Khan, T. Nikšić, and D. Vretenar, *Nature* **487**, 341 (2012).
- [7] H. Mäntysaari, B. Schenke, C. Shen, and W. Zhao, *Physical Review Letters* **131**, 062301 (2023).
- [8] J. J. Thompson, *Proc. Royal Society A* **89**, 1 (1913).
- [9] A. Bohr and B. R. Mottelson, *Nuclear Structure V. II* (World Scientific Publishing Company, 1998).
- [10] R. H. Spear, *Phys. Rep.* **73**, 369 (1981).
- [11] M. Carchidi, B. H. Wildenthal, and B. A. Brown, *Phys. Rev. C* **34**, 2280 (1986).
- [12] R. R. Rodríguez-Guzmán, J. L. Egido, and L. M. Robledo, *Eur. Phys. J. A* **17**, 37–47 (2003).
- [13] E. F. Zhou, J. M. Yao, Z. P. Li, J. Meng, and P. Ring, *Phys. Lett. B* **753**, 227 (2016).
- [14] P. Marević, J. P. Ebran, E. Khan, T. Nikšić, and D. Vretenar, *Phys. Rev. C* **97**, 024334 (2018).
- [15] T. Matsuse, M. Kamimura, and Y. Fukushima, *Prog. Theor. Phys.* **53**, 706 (1975).
- [16] J. Le Bloas, N. Pillet, M. Dupuis, J. M. Daugas, L. M. Robledo, C. Robin, and V. G. Zelevinsky, *Phys. Rev. C* **89**, 011306 (2014).
- [17] I. Hamamoto, *Nucl. Phys.* **73**, 225 (1965).
- [18] J. Cerny, *Nuclear Spectroscopy and Reactions*, Nuclear Spectroscopy and Reactions No. pt. 2 (Academic Press, 1974).
- [19] J. de Boer and J. Eichler, in *Adv. Nucl. Phys.* (Springer, 1968) pp. 1–65.
- [20] J. N. Orce, *Int. J. Mod. Phys. E* **29**, 2030002 (2020).
- [21] O. Häusser, B. W. Hooton, D. Pelte, T. K. Alexander, and H. C. Evans, *Physical Review Letters* **22**, 359 (1969).
- [22] A. Christy and O. Häusser, *Nuclear Data Tables* **11**, 281 (1973).
- [23] M. P. Fewell, S. Hinds, D. C. Kean, and T. H. Zabel, *Nuclear Physics A* **319**, 214 (1979).
- [24] K. Nakai, F. S. Stephens, and R. M. Diamond, *Nucl. Phys. A* **150**, 114 (1970).
- [25] D. Schwalm, A. Bamberger, P. G. Bizzeti, B. Povh, G. A. P. Engelbertink, J. W. Olness, and E. K. Warburton, *Nucl. Phys. A* **192**, 449 (1972).
- [26] D. K. Olsen, A. R. Barnett, S. F. Biagi, N. H. Merrill, and W. R. Phillips, *Nucl. Phys. A* **220**, 541 (1974).
- [27] S. J. Q. Robinson, A. Escuderos, L. Zamick, P. v. Neumann-Cosel, A. Richter, and R. W. Fearick, *Phys. Rev. C* **73**, 037306 (2006).
- [28] S. Yeager and L. Zamick, arXiv preprint arXiv:0807.4679 (2008).
- [29] Y. Y. Sharon, N. Benczer-Koller, G. J. Kumbartzki, L. Zamick, and R. F. Casten, *Nucl. Phys. A* **980**, 131 (2018).
- [30] S. Raman, C. W. Nestor, and P. Tikkainen, *Atomic Data and Nuclear Data Tables* **78**, 1 (2001).
- [31] D. Schwalm, private communication (2000).
- [32] J. Leske, K. H. Speidel, O. Kenn, S. Schielke, G. Müller, J. Gerber, N. Benczer-Koller, G. Kumbartzki, and P. Maier-Komor, *Phys. Lett. B* **551**, 249 (2003).
- [33] “XIA,” Available online from: <https://xia.com> (2024).
- [34] “Micron semiconductors,” <https://www.micronsemiconductor.co.uk/multi-element-detectors-double-sided> (2024).
- [35] A. N. Ostrowski, S. Cherubini, T. Davinson, D. Groombridge, A. M. Laird, A. Musumarra, A. Ninane, A. C. Shotter, and P. J. Woods, *Nucl. Instrum. Methods Phys. Res. A* **480**, 448 (2002).
- [36] J. F. Sharpey-Schafer, *Nucl. Phys. News* **14**, 3 (2004).
- [37] T. Czosnyka, D. Cline, and C. Wu, *Bull. Am. Phys. Soc* **28**, 745 (1983).
- [38] M. Zielińska, L. P. Gaffney, K. Wrzosek-Lipska, E. Clément, T. Grahn, N. Kesteloot, P. Napiorkowski, J. Pakarinen, P. Van Duppen, and W. N., *Eur. J. Phys. A* **52**, 1 (2016).
- [39] J. F. Ziegler, M. D. Ziegler, and J. P. Biersack, *Nuclear Instruments and Methods in Physics Research Section B: Beam Interactions with Materials and Atoms* **268**, 1818 (2010), 19th International Conference on Ion Beam Analysis.
- [40] D. R. Tilley, H. R. Weller, and G. M. Hale, *Nucl. Phys. A* **541**, 1 (1992).
- [41] C. Y. Wu, D. Cline, T. Czosnyka, A. Backlin, C. Bakta, R. M. Diamond, G. D. Dracoulis, L. Hasselgren, H. Kluge, B. Kotlinski, *et al.*, *Nucl. Phys. A* **607**, 178 (1996).
- [42] <https://bricc.anu.edu.au/> (2020).
- [43] A. Ekström, J. Cederkäll, D. D. DiJulio, C. Fahlander, M. Hjorth-Jensen, A. Blazhev, B. Bruyneel, P. A. Butler, T. Davinson, J. Eberth, C. Fransen, K. Geibel, H. Hess, O. Ivanov, J. Iwanicki, O. Kester, J. Kownacki, U. Köster, B. A. Marsh, P. Reiter, M. Scheck, B. Siebeck, S. Siem, I. Stefanescu, H. K. Toft, G. M. Tveten, J. Van de Walle, D. Voulot, N. Warr, F., K. Wrzosek, and M. Zielińska, *Phys. Rev. C* **80**, 054302 (2009).
- [44] B. Pritychenko, M. Birch, B. Singh, and M. Horoi, *Atomic Data and Nuclear Data Tables* **107**, 1 (2016).
- [45] P. Petkov, C. Müller-Gatermann, D. Werner, A. Dewald, A. Blazhev, C. Fransen, J. Jolie, S. Ohkubo, and K. O. Zell, *Phys. Rev. C* **100**, 024312 (2019).
- [46] J. Eichler, *Phys. Rev.* **133**, B1162 (1964).
- [47] K. Alder and A. Winter, *Electromagnetic excitation* (North-Holland Publishing Company, Amsterdam-

- Oxford, 1975).
- [48] J. N. Orce, T. E. Drake, M. K. Djongolov, P. Navrátil, S. Triambak, G. C. Ball, H. Al Falou, R. Churchman, D. S. Cross, P. Finlay, C. Forssén, A. B. Garnsworthy, P. E. Garrett, G. Hackman, A. B. Hayes, R. Kshetri, J. Lassen, K. G. Leach, R. Li, J. Meissner, C. J. Pearson, E. T. Rand, F. Sarazin, S. K. L. Sjue, M. A. Stoyer, C. S. Sumithrarachchi, C. E. Svensson, E. R. Tardiff, A. Teigelhoefer, S. J. Williams, J. Wong, and C. Y. Wu, Phys. Rev. C **86**, 041303 (2012).
- [49] B. L. Berman and S. C. Fultz, Rev. Mod. Phys. **47**, 713 (1975).
- [50] G. Brown and M. Bolsterli, Physical Review Letters **3**, 472 (1959).
- [51] J. S. Levinger, *Nuclear Photo-Disintegration* (Oxford University Press, Oxford, 1960).
- [52] A. Migdal, J. Phys. Acad. Sci. USSR **8**, 331 (1944).
- [53] J. S. Levinger, Phys. Rev. **107**, 554 (1957).
- [54] T. E. Drake, “Winther-de boer coulomb-excitation code,” unpublished (1991).
- [55] C. Ngwetsheni and J. N. Orce, Phys. Lett. B **792**, 335 (2019).
- [56] C. Ngwetsheni and J. N. Orce, Hyp. Int. **24**, 94 (2019).
- [57] C. Ngwetsheni and J. N. Orce, EPJ Web of Conferences **223** (2019).
- [58] A. N. Gorbunov, V. A. Dubrovina, V. A. Osipova, V. S. Silaeva, and P. A. Cerenkov, SOVIET PHYSICS JETP **15** (1962).
- [59] S. Costa, C. Schaerf, and E. M. I. C. for Scientific Culture, *Photonuclear Reactions: Proceedings of the First Course of the International School on Electro and Photonuclear Reactions, Erice, 2-17 June 1976*, Lecture notes in physics No. v. 2 (Springer-Verlag, 1977).
- [60] J. N. Orce, At. Data Nucl. Data Tables **146**, 101511 (2022).
- [61] A. P. Komar, J. Exptl. Theoret. Phys. USSR **32**, 614 (1957).
- [62] J. M. Blatt and V. F. Weisskopf, *Theoretical nuclear physics* (Springer Science & Business Media, 2012).
- [63] J. N. Orce, C. Ngwetsheni, and B. A. Brown, Phys. Rev. C **108**, 044309 (2023).
- [64] B. A. Brown, A. Etchegoyen, W. D. M. Rae, and N. S. Godwin, MSU-NSCL Report **524** (1988).
- [65] E. Warburton and B. A. Brown, Physical Review C **46**, 923 (1992).
- [66] J. N. Orce and C. Ngwetsheni, J. Phys. G **51**, 075105 (2023).
- [67] O. Häusser, A. McDonald, T. Alexander, A. Ferguson, and R. Warner, Nucl. Phys. A **212**, 613 (1973).
- [68] F. C. Barker, Aust. J. Phys. **35**, 291 (1982).
- [69] M. K. Raju, J. N. Orce, P. Navrátil, G. C. Ball, T. E. Drake, S. Triambak, G. Hackman, C. J. Pearson, K. J. Abrahams, E. H. Akakpo, *et al.*, Phys. Lett. B **777**, 250 (2018).
- [70] W. A. Richter, S. Mkhize, and B. A. Brown, Phys. Rev. C **78**, 064302 (2008).
- [71] J. Orce, E. M. Montes, K. Abrahams, C. Ngwetsheni, B. Brown, M. K. Raju, C. Mehl, M. Mokgolobotho, E. Akakpo, D. Mavela, *et al.*, Physical Review C **104**, L061305 (2021).
- [72] H. Hergert, S. Bogner, T. Morris, A. Schwenk, and K. Tsukiyama, Physics Reports **621**, 165 (2016), memorial Volume in Honor of Gerald E. Brown.
- [73] S. R. Stroberg, H. Hergert, S. K. Bogner, and J. D. Holt, Annual Review of Nuclear and Particle Science **69**, 307 (2019), <https://doi.org/10.1146/annurev-nucl-101917-021120>.
- [74] K. Tsukiyama, S. K. Bogner, and A. Schwenk, Phys. Rev. C **85**, 061304 (2012).
- [75] S. K. Bogner, H. Hergert, J. D. Holt, A. Schwenk, S. Binder, A. Calci, J. Langhammer, and R. Roth, Phys. Rev. Lett. **113**, 142501 (2014).
- [76] S. R. Stroberg, A. Calci, H. Hergert, J. D. Holt, S. K. Bogner, R. Roth, and A. Schwenk, Phys. Rev. Lett. **118**, 032502 (2017).
- [77] K. Hebeler, S. K. Bogner, R. J. Furnstahl, A. Nogga, and A. Schwenk, Phys. Rev. C **83**, 031301 (2011).
- [78] J. Simonis, K. Hebeler, J. D. Holt, J. Menéndez, and A. Schwenk, Phys. Rev. C **93**, 011302 (2016).
- [79] J. Simonis, S. R. Stroberg, K. Hebeler, J. D. Holt, and A. Schwenk, Phys. Rev. C **96**, 014303 (2017).
- [80] T. D. Morris, J. Simonis, S. R. Stroberg, C. Stumpf, G. Hagen, J. D. Holt, G. R. Jansen, T. Papenbrock, R. Roth, and A. Schwenk, Phys. Rev. Lett. **120**, 152503 (2018).
- [81] S. R. Stroberg, J. D. Holt, A. Schwenk, and J. Simonis, Phys. Rev. Lett. **126**, 022501 (2021).
- [82] A. Ekström, G. R. Jansen, K. A. Wendt, G. Hagen, T. Papenbrock, B. D. Carlsson, C. Forssén, M. Hjorth-Jensen, P. Navratil, and W. Nazarewicz, Phys. Rev. C **91**, 051301 (2015).
- [83] E. Leistenschneider, M. P. Reiter, S. Ayet San Andrés, B. Koote, J. D. Holt, P. Navrátil, C. Babcock, C. Barbieri, B. R. Barquest, J. Bergmann, J. Bollig, T. Brunner, E. Dunling, A. Finlay, H. Geissel, L. Graham, F. Greiner, H. Hergert, C. Hornung, C. Jesch, R. Klawitter, Y. Lan, D. Lascar, K. G. Leach, W. LipPERT, J. E. McKay, S. F. Paul, A. Schwenk, D. Short, J. Simonis, V. Somà, R. Steinbrügge, S. R. Stroberg, R. Thompson, M. E. Wieser, C. Will, M. Yavor, C. Andreoiu, T. Dickel, I. Dillmann, G. Gwinner, W. R. Plaß, C. Scheidenberger, A. A. Kwiatkowski, and J. Dilling, Phys. Rev. Lett. **120**, 062503 (2018).
- [84] R. P. De Groote, J. Billowes, C. L. Binnersley, M. L. Bissell, T. E. Cocolios, T. Day Goodacre, G. J. Farooq-Smith, D. V. Fedorov, K. T. Flanagan, S. Franchoo, *et al.*, Nature Physics **16**, 620 (2020).
- [85] R. P. De Groote, J. Billowes, C. L. Binnersley, M. L. Bissell, T. E. Cocolios, T. Day Goodacre, G. J. Farooq-Smith, D. V. Fedorov, K. T. Flanagan, S. Franchoo, *et al.*, Nature Physics **16**, 620 (2020).
- [86] N. M. Parzuchowski, S. R. Stroberg, P. Navrátil, H. Hergert, and S. K. Bogner, Phys. Rev. C **96**, 034324 (2017).
- [87] R. F. Garcia Ruiz, M. L. Bissell, K. Blaum, N. Frömmgen, M. Hammen, J. D. Holt, M. Kowalska, K. Kreim, J. Menéndez, R. Neugart, G. Neyens, W. Nörterhäuser, F. Nowacki, J. Papuga, A. Poves, A. Schwenk, J. Simonis, and D. T. Yordanov, Phys. Rev. C **91**, 041304 (2015).
- [88] J. Henderson, G. Hackman, P. Ruotsalainen, S. Stroberg, K. Launey, J. Holt, F. Ali, N. Bernier, M. Bentley, M. Bowry, *et al.*, Physics Letters B **782**, 468 (2018).
- [89] A. Klose, K. Minamisono, A. J. Miller, B. A. Brown, D. Garand, J. D. Holt, J. D. Lantis, Y. Liu, B. Maaf, W. Nörterhäuser, S. V. Pineda, D. M. Rossi, A. Schwenk, F. Sommer, C. Sumithrarachchi, A. Teigelhöfer, and J. Watkins, Phys. Rev. C **99**, 061301 (2019).
- [90] S. Heil, M. Petri, K. Vobig, D. Bazin, J. Belarge,

- P. Bender, B. Brown, R. Elder, B. Elman, A. Gade, T. Haylett, J. Holt, T. Hüther, A. Hufnagel, H. Iwasaki, N. Kobayashi, C. Loelius, B. Longfellow, E. Lunderberg, M. Mathy, J. Menéndez, S. Paschalis, R. Roth, A. Schwenk, J. Simonis, I. Syndikus, D. Weisshaar, and K. Whitmore, Phys. Lett. B **809**, 135678 (2020).
- [91] C. Sarma and P. C. Srivastava, Journal of Physics G: Nuclear and Particle Physics **50**, 045105 (2023).
- [92] J. Henderson, G. Hackman, P. Ruotsalainen, J. D. Holt, S. R. Stroberg, C. Andreoiu, G. C. Ball, N. Bernier, M. Bowry, R. Caballero-Folch, S. Cruz, A. Diaz Varela, L. J. Evitts, R. Frederick, A. B. Garnsworthy, M. Holl, J. Lassen, J. Measures, B. Olaizola, E. O'Sullivan, O. Paetkau, J. Park, J. Smallcombe, C. E. Svensson, K. Whitmore, and C. Y. Wu, Phys. Rev. C **105** (2022), 10.1103/physrevc.105.034332.
- [93] A. Magilligan and B. A. Brown, Phys. Rev. C **101**, 064312 (2020).
- [94] M. Bender, P.-H. Heenen, and P.-G. Reinhard, Rev. Mod. Phys. **75**, 121 (2003).
- [95] T. Nikšić, D. Vretenar, and P. Ring, Prog. Part. Nucl. Phys. **66**, 519 (2011).
- [96] L. M. Robledo, T. R. Rodríguez, and R. R. Rodríguez-Guzmán, J. Phys. G: Nuclear and Particle Physics **46**, 013001 (2018).
- [97] N. Schunck, ed., *Energy Density Functional Methods for Atomic Nuclei*, 2053-2563 (IOP Publishing, 2019).
- [98] G. A. Lalazissis, T. Nikšić, D. Vretenar, and P. Ring, Phys. Rev. C **71**, 024312 (2005).
- [99] J. Meng, H. Toki, S.-G. Zhou, S. Q. Zhang, W. H. Long, and L. S. Geng, Prog. Part. Nucl. Phys. **57**, 470 (2006).
- [100] T. Nikšić, D. Vretenar, and P. Ring, Phys. Rev. C **78**, 034318 (2008).
- [101] Y. Tian, Z. Y. Ma, and P. Ring, Phys. Lett. B **676**, 44 (2009).
- [102] D. L. Hill and J. . A. Wheeler, Phys. Rev. **89**, 1102 (1953).
- [103] P. Marević, *Towards a unified description of quantum liquid and cluster states in atomic nuclei within the relativistic energy density functional framework*, Theses, Université Paris Saclay (COmUE) (2018).
- [104] J. Dobaczewski, W. Nazarewicz, and P. G. Reinhard, Journal of Physics G: Nuclear and Particle Physics **41**, 074001 (2014).
- [105] J. D. McDonnell, N. Schunck, D. Higdon, J. Sarich, S. M. Wild, and W. Nazarewicz, Phys. Rev. Lett. **114**, 122501 (2015).
- [106] M. Frosini, T. Duguet, J.-P. Ebran, B. Bally, H. Herger, T. R. Rodríguez, R. Roth, J. M. Yao, and V. Somà, Eur. Phys. J. A **58**, 64 (2022).
- [107] D. Lee, private communication (2024).